Journal of Physics: Conference Series

Effects of Zn doping on the pinning potential and the glass-liquid transition temperature of $YBa_2Cu_3O_{6+\delta}$ films

Effects of Zn doping on the pinning potential and the glass-liquid transition temperature of $YBa_2Cu_3O_{6+\delta}$ films

Kai Ackermann, Vadim Mai, Jens Hänisch and Bernhard Holzapfel

Karlsruhe Institute of Technology, Institute for Technical Physics, Hermann-von-Helmholtz-Platz 1, 76344 Eggenstein-Leopoldshafen

E-Mail: kai.ackermann@kit.edu

Abstract. A pristine $YBa_2Cu_3O_{6+\delta}$ film as well as two Zn-doped $YBa_2(Cu_{1-x}Zn_x)_3O_{6+\delta}$ films with doping levels x of 0.2 % and 0.4 %, respectively, grown epitaxially on $SrTiO_3$ single crystalline substrates by pulsed laser deposition, were investigated regarding the effect of the doping on the glass-liquid transition line and the pinning potential distribution. Zn doping did not show any effect on the shape of the transition line but caused a suppression of the transition temperature T_{GL} of about $16\,K\%^{-1}$. Although the doping did not lead to an additional pinning effect, the increase of the critical current density j_c towards lower temperatures is mainly driven by the variation of the threshold critical current density, j_{cm}. The width of the critical current density distribution j_0 saturates at low temperatures and only drops above $\sim 0.9\,T_{GL}$.

1. Introduction

Since Fisher and Koch et al. [1,2] introduced the vortex glass theory, many investigations, e.g. [3,4,5], were performed to understand the vortex dynamics in the class of *RE*BCO compounds. As has been shown, impurity doping with Zn as well as oxygen deficiency strongly influences the disorder transition in bulk samples [6,7]. The transition line moves towards lower fields with increasing impurity concentration until the Bragg-glass phase vanishes completely. This can be explained with an increased pinning energy U_p resulting in an increased ratio U_p/U_e with U_e being the elastic energy of the flux lines. Furthermore, it indicates a high density of growth-related defects like atomic vacancies, dislocations, or stacking faults in *RE*BCO films since a disorder transition or Bragg-glass phase could not be observed in such films so far. This implies that it is crucial for the understanding of artificial pinning in *RE*BCO films to analyse how impurity doping influences the film properties within the vortex-glass phase. Therefore, many investigations, e.g. [8,9,10], studied the influence of artificial pinning centres on the critical current density, critical temperature, and charge carrier density. However, in view of a broad range of superconducting power applications, the development of custom-designed pinning landscapes requires a model how impurities influence the underlying pinning potential U_p and the corresponding critical current density distribution $P(j_c)$.

For that reason, we studied the effect of Zn doping on $P(j_c)$ of $YBa_2Cu_3O_{6+\delta}$ films by analysing measured voltage-current curves $U(I)_{B,T}$ using the percolation theory introduced by Yamafuji and Kiss [11,12]. It well describes the concave shape of the $\ln(U) - \ln(I)$ curves in the vortex glass phase near the glass-liquid transition [13]. The electric field-current density, $E - j$, characteristic is given by equation 1 [7] and can be obtained from the assumed $P(j_c)$ distribution. It gives access to the relevant parameters of the distribution.

$$E(j) = \frac{\rho_f j}{m_0 + 1}\left(\frac{j}{j_0}\right)^{m_0}\left(1 - \frac{j_{cm}}{j}\right)^{m_0+1} \qquad T \leq T_{GL} \qquad (1)$$

The parameter j_{cm} is the threshold critical current density, which means that for $j < j_{cm}$ all pinning centres are active. j_0 is related to the width of $P(j_c)$, while m_0 determines its shape. m_0 is related to the dynamic critical index z, which is known from the scaling of $E - J$ curves according to the vortex glass theory. The remaining parameter ρ_f is the flux flow resistivity which can be calculated by measuring the normal state resistivity ρ_n via equation 2 [14].

$$\rho_f = \frac{B}{B_{c2}}\rho_n \qquad B \ll B_{c2} \qquad (2)$$

2. Experimental

Epitaxial $YBa_2(Cu_{1-x}Zn_x)_3O_{6+\delta}$ films with a nominal zinc content x ranging from 0.0 % to 0.4 % have been grown on (001)-oriented single crystalline $SrTiO_3$ substrates with dimensions of $10\,mm \times 10\,mm \times 1\,mm$. The films were deposited by on-axis pulsed laser deposition at 10 Hz using a frequency-tripled Nd:YAG laser ($\lambda = 355\,nm$, Quanta-Ray Indi-40-10, Spectra-Physics). For that purpose, three polycrystalline targets pressed uniaxially at 100 MPa with different Zn content were prepared from a stoichiometric mixture of Y_2O_3, $BaCO_3$, CuO and ZnO powders. Afterwards the targets were calcinated and sintered in air at 890 °C and 950 °C, respectively. The substrates were glued on a resistive heater from Twente Solid State Technology whose temperature was measured with a type K thermocouple. The deposition temperature was kept constant at 800 °C, and an oxygen flow of $1\,l min^{-1}$ at a pressure of 300 Pa was applied. The laser energy was kept constant at around 100 mJ which corresponds to a laser fluence ϵ of $3.2\,J cm^{-2}$. After deposition, the films were annealed at 450 °C for 1 h in a tube furnace under oxygen flow of $1\,l min^{-1}$ at ambient pressure.

Surface morphology and in-plane and out-of-plane texture were investigated with a Bruker Dimension Edge atomic force microscope (AFM), a Zeiss Leo 1350 scanning electron microscope (SEM) and a Bruker D8 Discover X-Ray diffractometer. The AFM height and adhesion maps were obtained with ScanAsyst-Air Si/Si_3N_4 tips ($f = 70\,kHz, l = 0.4\,N m^{-1}$) at a scan rate between 0.1 Hz and 0.3 Hz. The X-Ray diffractometer was equipped with a Cu X-Ray tube and operated at 40 kV and 40 mA.

$U(I)_{B,T}$ and $U(T)_{I,B}$ characteristics were measured in a physical properties measurement system from Quantum Design. Instead of the build-in system bridge, a Keithley 2460 SourceMeter was used in combination with a Keithley 2182A nanovoltmeter for pulsed current measurements. To reduce the noise level and thereby to increase the measurable electric field range, meander-shaped bridges of 136.5 mm length and 100 µm width were structured chemically using the AZ 5214 E photoresist from Merck and a 1 % HNO_3 solution. In addition, short bridges with a length of 0.5 mm on the same samples were used to determine the critical current density with an electric field criterion of $1\,\mu V cm^{-1}$.

3. Results and discussion

Step height measurements of the structured $YBa_2(Cu_{1-x}Zn_x)_3O_{6+\delta}$ samples revealed a slight increase of the film thickness and the growth rate towards higher Zn doping levels. We determined an average thickness of about 361 nm for the pristine, 395 nm for the 0.2 % and 404 nm for the 0.4 % doped sample. This corresponds to an increase of the growth rate from 0.6 Å for the pristine film to 0.675 Å per pulse at $x = 0.4\,\%$. As AFM images reveal, the density of large precipitates on the sample surface decreases while their size is increased in the doped samples, Figure 1. EDX measurements confirmed that most of these precipitates are secondary phases, especially CuO or CuO_2, which is in good agreement with previous investigations [15,16]. On the other hand, the density of small surface defects strongly increases. However, XRD $\theta - 2\theta$ and φ scans as well as AFM measurements of all samples do not show any indications for misoriented grains.

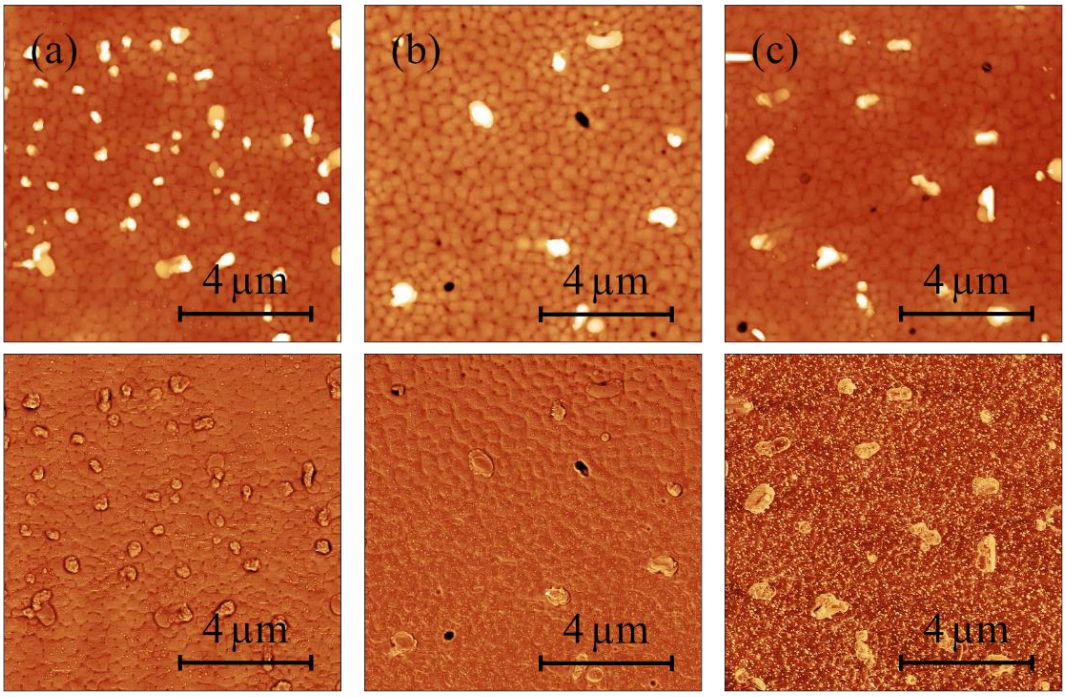

Figure 1. AFM height and adhesion maps of the (a) pristine, (b) 0.2 % and (c) 0.4 % Zn doped sample.

To determine the glass-liquid transition temperature T_{GL}, we measured $U(I)_{B,T}$ characteristics at magnetic field values between 2 T and 14 T over a broad temperature range with a step size of 1 K. As predicted by the vortex glass theory, the $\ln(E) - \ln(j)$ plots showed a convex shape above, a concave shape below and a constant slope at T_{GL}. As expected, T_{GL} obtained with this analysis shifts to lower temperatures with increasing Zn doping, Figure 2. On average, the suppression of T_{GL} by Zn doping was $16\,\mathrm{K}\%^{-1}$. This value is about $4\,\mathrm{K}\%^{-1}$ higher than the values reported in former publications [17,18] but might be explained by the increased inhomogeneity along the meander structure compared to small bridges. However, the obtained T_{GL} values are in good agreement with resistive T_{c} measurements which show just a small deviation of about 1.5 K towards higher temperatures. The glass-liquid transition line shows a constant slope which indicates a homogeneous distribution of Zn atoms without any formation of nanocolumnar defects parallel to the $\boldsymbol{c}$ axes.

Critical current density measurements revealed comparable j_{c} values for all three samples over the measured magnetic field range, Figure 3. Although the values in the pristine sample are slightly higher compared to those in doped samples, the deviation is less than 25 %. However, we expected much higher j_{c} values in the doped samples especially at high fields since earlier studies on sputtered films revealed an optimal doping level of about 0.2 % [19]. Nevertheless, the measurements at 25 K and $x = 0.4\,\%$ show a decreased deviation towards higher fields which might indicate a crossover above 14 T. According to Tomé-Rosa et al. [19], this crossover field is decreasing towards higher doping levels before it increases again due to the influence of T_{c} suppression. This might indicate that the doping levels of our samples were too low to show strong artificial pinning.

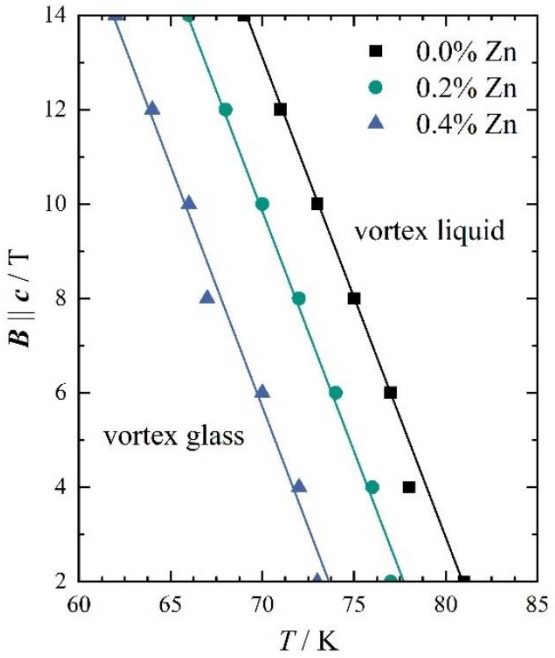

Figure 2. Dependence of the glass-liquid transition line on the Zn concentration. The values of T_{GL} were optained from $\ln(U) - \ln(I)$ measurements at constant B and T with constant slope.

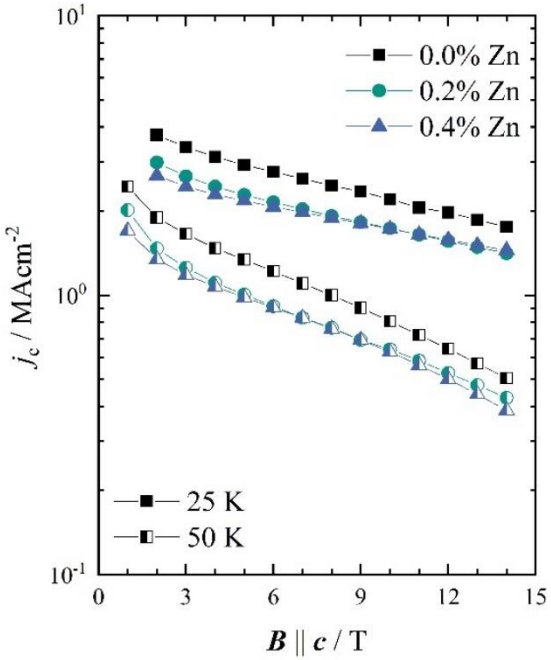

Figure 3. Critical current density $j_{\mathrm{c}}(B)$ of doped and undoped samples at two temperatures. The j_{c} values were determined from $E(j)_{B,T}$ measurements using an electric field criterion of $1\,\mu\mathrm{Vcm}^{-1}$.

To analyse how the parameters j_0 and j_{cm} of the pinning potential evolve towards lower temperatures, measured $E(j)_{B,T}$ were fitted according to equation 1. The flux flow resistivity was calculated from measured values of ρ_{n} using B_{c2} values determined by Sekitani et al. [20]. First of all, we obtained similar values for j_0 and j_{cm} for all three samples. This fits to the results of the j_{c} measurements since j_{c} should be in the range of $j_{\mathrm{k}} = j_{\mathrm{cm}} + j_0$. Furthermore, the comparable values of j_0 indicate a small pinning efficiency of the Zn atoms at such low concentrations, because $P(j_{\mathrm{c}})$ should be narrow in case of a single dominant pinning mechanism . As shown in figure 4, j_0 saturates towards lower temperatures. This is somehow expected because below a certain temperature almost all pinning centres should be active. On the other hand, the temperature range where this takes place seems to be rather small, since we only observe a strong decrease of j_0 above $\sim 0.9\,T_{\mathrm{GL}}$. Below this value, the increase of j_{c} is mainly driven by an increase of j_{cm} as shown in figure 5. Even for a constant ratio T/T_{GL}, j_{cm} drops strongly towards higher fields, while j_0 shows only a small decrease by a factor below 2.

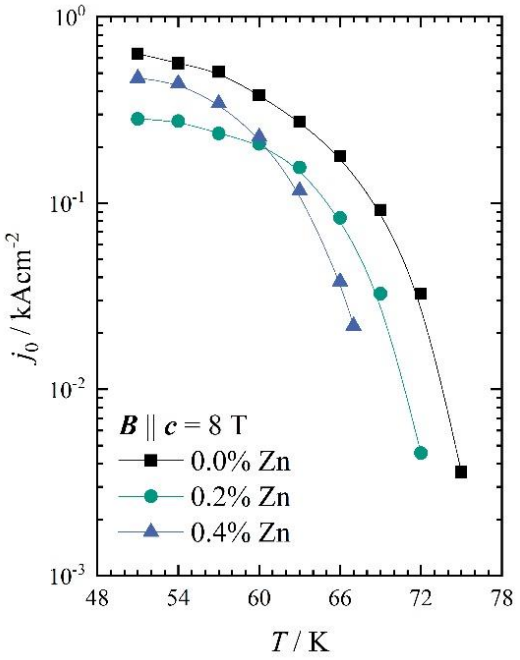

Figure 4. Temperature dependence of the width of the critical current density distribution j_0 at a magnetic field $B = 8\,\mathrm{T}$.

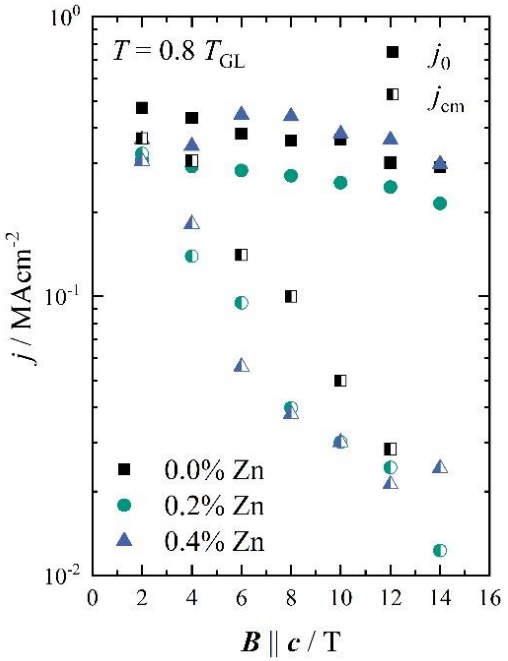

Figure 5. Magnetic field dependency of the threshold critical current density j_{cm} and the width of the critical current density distribution j_0 at $0.8\,T_{\mathrm{GL}}$.

4. Conclusion

In summary, we have grown smooth and highly oriented $YBa_2(Cu_{1-x}Zn_x)_3O_{6+\delta}$ films with doping levels x ranging from 0.0 % to 0.4 %. In doped samples, a reduced density of metal-oxide precipitates with reduced average size was observed. Measurements of the glass-liquid transition temperature T_{GL} revealed a slightly higher suppression of T_{c} of $16\,\mathrm{K\%^{-1}}$ than reported in the literature, which might be explained by an increased inhomogeneity along the meander structure or a deviation of the Zn concentration between target and film. Further, reasonable values of j_{c} were obtained in all samples, although we could not observe any additional pinning effect. Nevertheless, the analysis of the pinning potential distribution revealed a saturation of its width j_0 towards lower temperatures. This shows that almost all pinning centres in pristine films are active below $0.9\,T_{\mathrm{GL}}$. At lower temperatures, the increase of j_{c} is mainly driven by the increase of j_{cm}.

References

[1] Fisher M P A 1989 *Phys. Rev. Lett.* **62** 1415–8
[2] Koch R H, Foglietti V, Gallagher W J, Koren G, Gupta A and Fisher M P A 1989 *Phys. Rev. Lett.* **62** 1511–4
[3] Safar H, Foltyn S R, Jia Q X and Maley M P 1996 *Philos. Mag.* B **74** 647–54
[4] Kiss T, Matsushita T and Irie F 1999 *Supercond. Sci. Technol.* **12** 1079–82
[5] Li D and Rosenstein B 2003 *Phys. Rev. Lett.* **90** 167004
[6] Nishizaki T, Maeda M, Sato T and Kobayashi N 2005 *Physica* C **426–31** 18–22
[7] Matsushita T 2014 *Flux Pinning in Superconductors* vol 2 (Heidelberg: Springer) pp 324, 339
[8] Jha A K and Matsumoto K 2019 *Front Phys.* **7** 82
[9] Matsumoto K and Mele P 2009 *Supercond. Sci. Technol.* **23** 014001
[10] Obradors X, Puig T, Palau A, Pomar A, Sandiumenge F, Mele P and Matsumoto K 2011 Nanostructured superconductors with efficient vortex pinning *Comprehensive Nanoscience*

and Technology vol 3 ed Andrews D L, Scholes G D and Wiederrech G P (Amsterdam: Elsevier) pp 303–49
[11] Yamafuji K and Kiss T 1996 *Physica* C **258** 197–212
[12] Yamafuji K and Kiss T 1997 *Physica* C **290** 9–22
[13] Sirois F, Grilli F and Morandi A 2019 *IEEE Trans. Appl. Supercond.* **29** 8000110
[14] Kim Y B, Hempstead C F and Strnad A R 1965 *Phys. Rev.* **139**, A1163–72
[15] Eibl O and Roas B 1990 *J. Mater. Res.* **5** 2620–32
[16] Gong J P, Kawasaki M, Fujito K, Tsuchiya R, YoshimotoM and H. Koinuma 1994 *Phys. Rev.* B **50** 3280–87
[17] Veit M, Langen J, Galffy M, Jostarndt H D, Erle A, Blumenröder S, Schmidt H and Zirngiebl E 1988 *Physica* C **153–5** 900–1
[18] Tomé-Rosa C, Jakob G, Maul M, Walkenhorst A, Schmitt M, Wagner P, Przystupski P and Adrian H 1990 *Physica* C **171** 231–7
[19] Tomé-Rosa C, Jakob G, Paulson M, Wagner P, Walkenhorst A, Schmitt M and Adrian H 1991 *Physica* C **185-9** 2175–6
[20] Sekitani T, Miura N, Ikeda S, Matsuda Y H and Shiohara Y 2004 *Physica* B **346–7** 319–24